Chapter 2

Second- and Third-Order Statistical Characterization of Non-Linearity and Non-Gaussianity of Adult and Fetal ECG Signals and Noise

Walid A. Zgallai

Additional information is available at the end of the chapter

http://dx.doi.org/10.5772/52575

1. Introduction

This chapter investigates the application of digital signal processing techniques to ECG signals. The first few sections of this chapter are devoted to definitions and properties of cumulants, their spectra, and associated statistics. This is followed by describing the structural properties of the third-order cumulants of an adult male's chest ECG, maternal chest ECG, transabdominally-measured ECG, as well as fetal ECG signal using scalp-electrode. The non-linearity and non-stationarity of ECG signals are investigated using the bispectrum and bicoherence squared. The third-order cumulants, bispectra, and bicoherence squared of some noise components, namely, the baseline wander, electromyographic (EMG), and motion artefact noise isolated from the MIT/BIH databases are analysed. Finally, concluding remarks are discussed and summarised.

Adequate knowledge of the higher-order statistics (HOS) of both the maternal and fetal ECG signals must be acquired in order to pave the way for fetal QRS-complex identification and detection. There are several motivations behind using higher-order statistics in processing ECG signals. These motivations are:

i. ECG signals are predominantly non-Gaussian (Rizk et al., 1995; Rizk and Zgallai, 1999), and exhibit quadratic and higher-order non-linearities supported by third- and fourth-order statistics, respectively. It is worth mentioning that, in general, the third-order cumulants can support linear non-Gaussian, and non-linear signals.
ii. The maternal and fetal QRS-complex bispectral contours do not overlap with that of the baseline wander and that of the EMG above –20 dB normalised to the peak of the

maternal QRS-complex bispectrum (Zgallai, 2007). It is comparatively easy to detect and classify either using the bispectral contour template matching technique.

iii. In the HOS domain, the Gaussian noise diminishes if the data length is adequate (Nikias and Petropulu, 1993; Nam and Powers, 1994). This implies that it is possible, under certain conditions, to process the ECG signal in Gaussian noise-free domains. It was found (Rizk and Zgallai, 1999) that for ECG signals a minimum length of 1 sec is adequately long to suppress Gaussian noise in the higher-order statistical domains, whilst not long enough to violate Hinich's criterion of local stationarity (Brockett et al. 1988). Hinich tests for Gaussianity and linearity were performed on ECG signals (Zgallai, 2007). ECG signals are non-stationary in the statistical sense, but relatively short data can be successfully treated with conventional signal processing tools primarily designed for stationary signals. For example, when dealing with individual cardiac cycles, non-stationarity is not an issue but when one takes on board the heart rate time series which is chaotic and multi-dimensional then it is not wise to assume stationarity for analysis purposes (Rizk et al. 2002).

iv. In the third-order domain all sources of noise with symmetric probability density functions (pdfs), e.g., Gaussian and uniform, will vanish. The ECG signals are retained because they have non-symmetric distributions (Zgallai, et al., 1997).

v. ECG signals contain quadratic and cubic non-linearities (Rizk et al., 1998). Such measurable quantities of non-linearity if not synthesised and removed before any further processing for the purpose of signal identification and classification could lead to poor performance with regard to fetal QRS-complex detection rates.

An adaptive third-order Volterra structure (Nam and Powers, 1994) has been used to synthesise the linear, quadratic non-linear, and cubic non-linear components of ECG signals. The removal of non-linearities in the transabdominal ECG signal yields an increase in the fetal heartbeat detection rates by up to 7% in the third-order cumulant matching technique (Zgallai, 2010), and 10% in the bispectral contour template matching technique (Zgallai, 2012 a, Zgallai, 2012 b).

For noise identification and characterisation in the third-order statistical domain, use is made of the recorded normal ECG signals contained in the MIT/BIH databases (MIT/BIH, 1997). The third-order cumulants, bispectra, and bicoherence squared of some noise components, namely, the baseline wander, electromyographic (EMG) (Zgallai, 2009), and motion artefact noise isolated from the MIT/BIH databases are analysed. Knowing the statistics of those noise components, would facilitate the detection of ECG signals against a cocktail of background noise in either the cumulant or the bispectrum domain. Higher detection rate of fetal QRS-complex can be achieved in the enhanced fetal QRS-complex bispectrum domain against both maternal and motion artefact bispectral contribution (Zgallai, 2012 a). Bispectral enhancement has been carried out after removing the baseline wander, and in difficult cases, after linearisation (removing non-linearity from the noise contaminated maternal transabdominal signal).

2. Background and definitions

2.1. Cumulants

Given a set of n real variables {x_1, x_2, …, x_n}, their joint moments of order, r = k_1 + k_2 + … + k_n are given by (Kravtchenko-Berejnoi, V. et al. 1995):

$$Mom\ [x_1^{k_1}, x_2^{k_2}, \ldots, x_n^{k_n}] \stackrel{\nabla}{=} E\{x_1^{k_1}, x_2^{k_2}, \ldots, x_n^{k_n}\} = (-j)^r \left. \frac{\partial^r \phi(\omega_1, \omega_2, \ldots, \omega_n)}{\partial \omega_1^{k_1} \partial \omega_2^{k_2} \ldots \partial \omega_n^{k_n}} \right|_{\omega_1 = \omega_2 = \ldots = \omega_n = 0} \quad (1)$$

where $\phi(\omega_1, \omega_2, \ldots, \omega_n) \stackrel{\nabla}{=} E\{e^{j(\omega_1 x_1, \omega_2 x_2, \ldots, \omega_n x_n)}\}$ is their joint characteristic function. E{.} denotes the expectation operator. Another form of the joint characteristic function is defined as the natural logarithm of $\phi(\omega_1, \omega_2, \ldots, \omega_n)$, i.e., (Nikias and Petropulu, 1993)

$$\tilde{\Psi}(\omega_1, \omega_2, \ldots, \omega_n) \stackrel{\nabla}{=} \ln[\phi(\omega_1, \omega_2, \ldots, \omega_n)] \quad (2)$$

For Gaussian processes, the logarithm of the characteristic function is a polynomial of degree two. Hence, all cumulants of order three and higher will be identically zero. The joint cumulants of order r of the same set of random variables, are defined as the coefficients in the Taylor expansion of the second characteristic function about zero, i.e., (Nikias and Petropulu, 1993)

$$Cum\ [x_1^{k_1}, x_2^{k_2}, \ldots, x_n^{k_n}] \stackrel{\nabla}{=} E\{x_1^{k_1}, x_2^{k_2}, \ldots, x_n^{k_n}\} = (-j)^r \left. \frac{\partial^r \tilde{\Psi}(\omega_1, \omega_2, \ldots, \omega_n)}{\partial \omega_1^{k_1} \partial \omega_2^{k_2} \ldots \partial \omega_n^{k_n}} \right|_{\omega_1 = \omega_2 = \ldots = \omega_n = 0} \quad (3)$$

Thus, the joint can be expressed in terms of the joint moments of a set of random variables. The moments of the random variable {x_1} are defined as (Nikias and Petropulu, 1993)::

$$m_1 = E\{x_1\}.\ m_2 = E\{x_1^2\}.\ m_3 = E[x_1^3]. \quad (4)$$

Cumulants are related to moments by (Nikias and Petropulu, 1993)

$$c_1 = m_1.\ c_2 = m_2 - m_1^2.\ c_3 = m_3 - 3\, m_2 m_1 + 2\, m_1^3. \quad (5)$$

For three random variables x_1, x_2, and x_3 the third-order cumulants are defined as (Kravtchenko-Berejnoi, V. et al. 1995):

$$c_3^x(\tau_1, \tau_2) = m_3^x(\tau_1, \tau_2) - m_1^x\left[m_2^x(\tau_1) + m_2^x(\tau_2) + m_2^x(\tau_2 - \tau_1)\right] + 2 \cdot \left(m_1^x\right)^3 \quad (6)$$

2.2. Properties of cumulants

1. c [a_1x_1, a_2x_2, …, a_nx_n] = a_1a_2 … a_n c [x_1, x_2, …, x_n] (Nikias and Petropulu, 1993).

2. Cumulants are symmetric functions in their arguments, e.g., $c[x_1,x_2,x_3] = c[x_2,x_1,x_3] = c[x_3,x_2,x_1]$, and so on (Nikias and Petropulu, 1993)..
3. If the random variables $\{x_1, x_2, \ldots, x_n\}$ can be divided into any two or more groups which are statistically independent, their nth-order cumulant is identical to zero; i.e. $c[x_1, x_2, \ldots, x_n] = 0$, whereas in general $Mom[x_1, x_2, \ldots, x_n] \neq 0$ (Nikias and Petropulu, 1993)..
4. If the sets of random variables $\{x_1, x_2, \ldots, x_n\}$ and $\{y_1, y_2, \ldots, y_n\}$ are independent, then $c[x_1+y_1, x_2+y_2, \ldots, x_n+y_n] = c[x_1, x_2, \ldots, x_n] + c[y_1, y_2, \ldots, y_n]$ (Nikias and Petropulu, 1993).
5. If the set of random variables $\{x_1, x_2, \ldots, x_n\}$ is jointly Gaussian, then all the information about their distribution is contained in the cumulants of order $n \leq 2$. Therefore, all cumulants of order greater than two ($n > 2$) have no new information to provide. This leads to the fact that all joint cumulants of order $n > 2$ are identical to zero for Gaussian random vectors. Hence, the cumulants of order greater than two, in some sense, measure the non-Gaussian nature of a time series (Nikias and Petropulu, 1993).

2.3. One-dimensional third-order cumulant slices

Since higher-order cumulants and spectra are multi-dimensional functions, their computation may be impractical in some applications due to excessive crunching. This is caused by the large CPU time taken to calculate HOS functions, compared to SOS functions. It was suggested to use 1-d slices of multi-dimensional cumulants, and their 1-d Fourier transforms, as ways of extracting useful information from higher-order statistics of non-Gaussian stationary processes (Nagata, 1970). The third-order cumulants of a non-Gaussian process, {x(k)}, is given by (Nikias and Petropulu, 1993):

$$C_3^x(\tau_1,\tau_2) = c\{x(k), x(k+\tau_1), x(k+\tau_2)\}\ . \tag{7}$$

One-dimensional slices of $C_3^x(\tau_1,\tau_2)$ can be defined as (Nikias and Petropulu, 1993):

$$r_{2,1}^x(\tau) \underline{\underline{\nabla}} c\{x(k), x(k), x(k+\tau)\} = C_3^x(0,\tau) \tag{8}$$

and

$$r_{1,2}^x(\tau) \underline{\underline{\nabla}} c\{x(k), x(k+\tau), x(k+\tau)\} = C_3^x(\tau,\tau) \tag{9}$$

Define the following even and odd functions (Nikias and Petropulu, 1993):

$$s_{2,1}^x(\tau) \underline{\underline{\nabla}} \frac{1}{2}[r_{2,1}^x(\tau) + r_{1,2}^x(\tau)] \tag{10}$$

and

$$q_{2,1}^x(\tau) \underline{\underline{\nabla}} \frac{1}{2}[r_{2,1}^x(\tau) - r_{1,2}^x(\tau)] \tag{11}$$

A 1-d spectrum could be defined as (Nikias and Petropulu, 1993):

$$R_{2,1}^{x}(\omega)=\sum_{\tau=-\infty}^{\infty} r_{2,1}^{x}(\tau)e^{-j\omega t}=\sum_{\tau=-\infty}^{\infty}\{s_{2,1}^{x}(\tau)\cdot\cos(\omega\tau)-jq_{2,1}^{x}(\tau)\cdot\sin(\omega\tau)\} \tag{12}$$

2.4. Cumulant spectra

Higher order spectra are defined as the multi-dimensional Fourier transforms of the higher order statistics of the superimposed signals in the presence of noise (Nikias and Raghuveer, 1987; Rosenblatt, 1985; Brillinger, 1965). The nth-order cumulant spectrum of a process {x(k)} is defined as the (n-1)-dimensional Fourier transform of the nth-order cumulant sequence. The nth-order cumulant spectrum is thus defined as (Nikias and Petropulu, 1993):

$$C_n^x(\omega_1,\omega_2,\ldots,\omega_{n-1})=\sum_{\tau_1=-\infty}^{+\infty}\cdots\sum_{\tau_{n-1}=-\infty}^{+\infty}c_n^x(\tau_1,\tau_2,\cdots,\tau_{n-1})\;e^{-j(\omega_1\tau_1+\omega_2\tau_2+\ldots,\omega_n\tau_{n-1})}, \tag{13}$$

where

$$\left|\omega_1\right|\le\pi \qquad for \qquad i=1,2,\ldots n-1, \quad and \qquad \left|\omega_1+\omega_2+\ldots+\omega_{n-1}\right|\le\pi\ .$$

Special cases

1. Power spectrum (n = 2):

$$C_2^x(\omega)=\sum_{\tau=-\infty}^{+\infty}c_2^x(\tau)\;e^{-j(\omega\tau)} \tag{14}$$

where $c_2^x(\tau)$ is the covariance.

2. Bispectrum (n = 3):

$$C_3^x(\omega_1,\omega_2)=\sum_{\tau_1=-\infty}^{+\infty}\sum_{\tau_2=-\infty}^{+\infty}c_3^x(\tau_1,\tau_2)\;e^{-j(\omega_1\tau_1+\omega_2\tau_2)} \tag{15}$$

where $c_3^x(\tau_1,\tau_2)$ is the third-order cumulant. Conventional higher-order statistics (HOS) estimates are asymptotically unbiased and consistent (Nagata, 1970), and easy to implement using FFT-based methods. The ability to resolve harmonic components is limited by the uncertainty principle of the Fourier transform. There are numerous methods for polyspectra estimation based on parametric methods. MA models have been treated in (Nikias, 1988; Friedlander and Porat, 1988). Spectral estimation methods based on non-causal AR models were developed in (Huzi, 1981). Methods based on ARMA models have been published (Lii, 1982). MA, AR and ARMA methods based on higher-order statistics were described (Mendel, 1988). A review of cumulant spectra and the asymptotic properties of their estimators were given in (Rosenblatt, 1983). Practical considerations for bispectral estimation were given (Subba Rao, 1983). The relationship between the bispectrum and conventional methods for their estimation was discussed (Zurbenko, 1982).

2.5. Non-stationarity and the OT region of the bispectrum

The bispectrum of a stationary sampled process must be zero in the triangle region OT, i.e., the region defined by the triangle, OT = $\{\omega_1, \omega_2 : \omega_2 \leq \omega_1, \pi \leq \omega_1 + \omega_2 \leq 2\pi - \omega_1\}$. The bispectrum in the OT region will be non-zero if the process is non-stationary. The bispectrum has 12 symmetric regions. The knowledge of the bispectrum in one triangular region is enough for a complete description of the bispectrum of a real process.

2.6. Nth-order coherency function

A normalised cumulant spectrum or the nth-order coherency index is a function that combines the cumulant spectrum of order n and the power spectrum. It is defined as (Nikias and Petropulu, 1993)

$$P_n^x(\omega_1, \omega_2, \ldots, \omega_{n-1}) \nabla = \frac{C_n^x(\omega_1, \omega_2, \ldots, \omega_{n-1})}{[C_2^x(\omega_1).C_2^x(\omega_2)\cdots C_2^x(\omega_{n-1}).C_2^x(\omega_1 + \omega_2 + \ldots + \omega_{n-1})]^2}. \quad (16)$$

The third-order (n = 3) coherence index is also called bicoherence. The nth order coherence index is useful for the detection and characterisation of non-linearities in time series via phase relations of their harmonic components. The coherency index is used to differentiate between linear non-Gaussian processes and non-linear processes when both have non-zero cumulants. If the coherency index is zero, then the process is linear and Gaussian. If the n^{th} order coherency index is not frequency dependent, then the process is linear non-Gaussian. If the coherency index is frequency dependent, then the process is non-linear (Nikias and Petropulu, 1993).

2.7. Statistical measures

A statistical measure could be described as an unbiased estimate when the expected value of the estimated statistic is, asymptotically, equal to the true value. An estimate of the cumulant spectra is unbiased if

$$E\left|\hat{C}_3^x(\omega_1, \omega_2)\right| = C_3^x(\omega_1, \omega_2) \quad (17)$$

The bias is defined as the difference between the true value and the expected value.

3. Second-order statistics of ECG signals

3.1. The probability density functions (pdfs) of ECG signals

Three essential ECG signals are considered:

1. the maternal chest ECG signal. This is measured using one surface electrode positioned on the chest and one reference electrode on the thigh;

2. The transabdominally-measured ECG signal which contains both maternal and fetal contributions amongst other deterministic and chaotic signals plus noise artefacts (Rizk et al., 2002). This is acquired using twin surface electrodes positioned near the mother's umbilicus and synchronised with the maternal chest signal;
3. the fetal scalp electrode ECG signal which will always be used as a reference signal in the assessment of any particular QRS detection technique based on non-invasive transabdominally-measured ECG signals. The non-symmetry of the probability density functions (pdfs) of the above mentioned signals is shown in the histograms of Fig. 1 and supports their third-order cumulants.

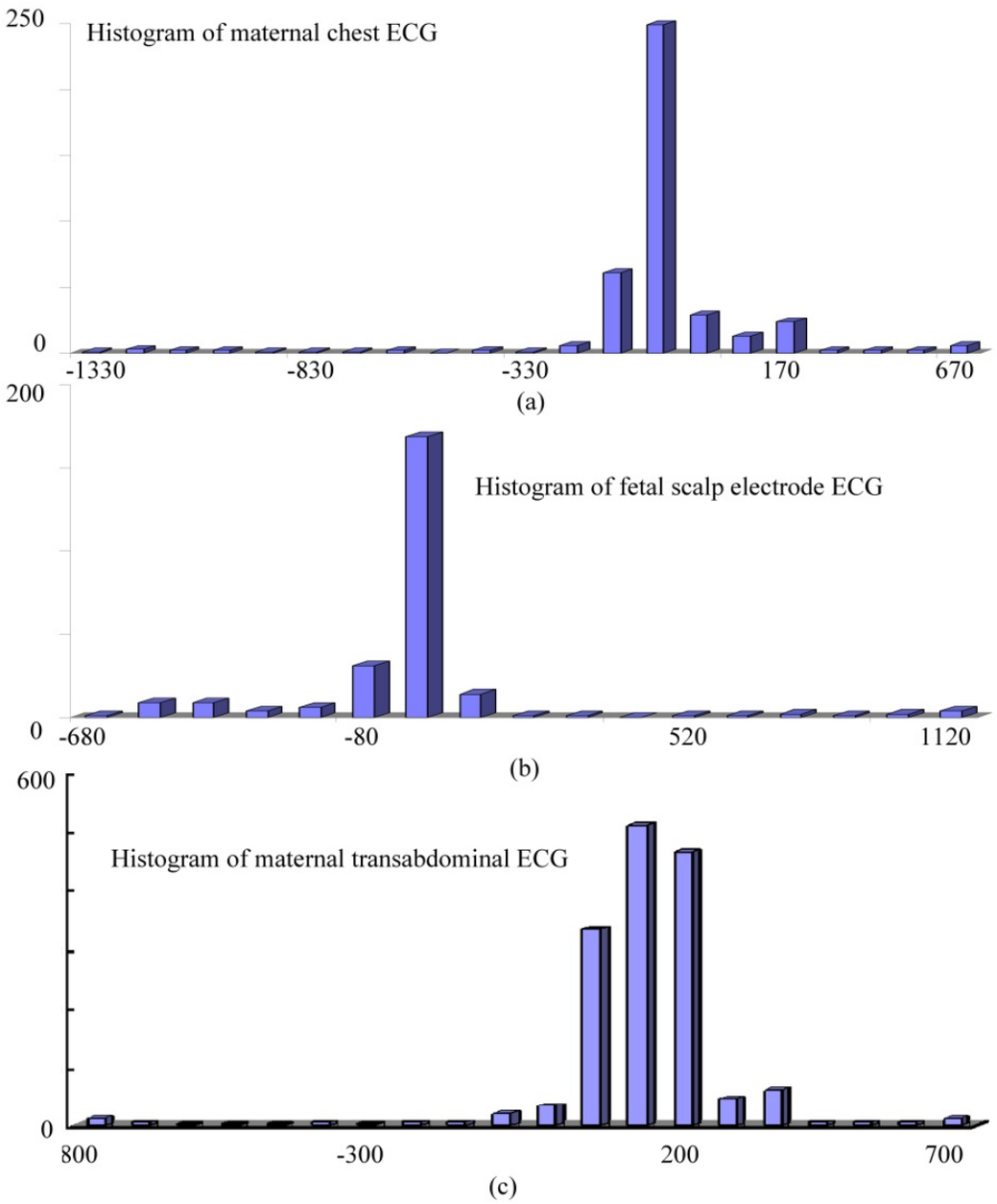

Figure 1. Histograms of typical templates of (a) a maternal chest ECG, (b) a fetal scalp electrode FECG, and (c) a maternal transabdominal ECG. They all show non-Gaussian distributions.

3.2. The second-order cumulants of ECG signals

Fig. 2 (a) shows a full maternal transabdominal cardiac cycle (1000 ms) which has been divided into four segments, I, II, III, and IV. These segments represent (I) the predominantly maternal QRS-complex, (II) the first fetal heartbeat with maternal contribution, (III) QRS-free ECG, and (IV) the second fetal heartbeat with maternal contribution, respectively. Fig. 2 (b) shows a typical example of the second-order cumulants (auto-correlation functions) for the segments shown in Fig. 2 (a). Second-order statistics do not show any distinguishable features that could be used to differentiate between maternal QRS-complex, fetal heartbeat with maternal contribution, and QRS-free ECG contributions.

3.3. The power spectrum of ECG signals

Fig. 3 depicts the power spectrum using the FFT method for (a) fetal scalp electrode ECG signal (data length 500 ms), (b) maternal transabdominal ECG (data length 1000 ms). The maternal cardiac cycle begins 50 ms before the R-wave and ends 50 ms before the next R-wave. The subject is at the first stage of labour (40 weeks gestation). The FFT method reveals a fetal scalp electrode ECG principal spectral peak at 30 Hz. The FFT method for the transabdominal cardiac cycle reveals the maternal principal spectral peak of 15 Hz. However, the FFT does not show fetal spectral peak from the segmented transabdominal signal. There is a shallow peak at 28 Hz and a shifted peak at 42 Hz (Zgallai, 2007).

4. Third-order statistics of ECG signals

4.1. Cumulants and their slices of cardiac cycles

The maternal chest ECG is measured using the standard three-lead electrode system. The maternal transabdominally-measured signals are obtained using two surface electrodes. The electrode pair is set over the umbilicus, and lined up with the median vertical axis of the uterus. The ground electrode is located on the woman's hip. The fetal scalp electrode is used when deemed necessary. Multi-dimensional Third-order cumulants TOCs were computed for the above ECG signals as well as for the four segments of the maternal transabdominal cardiac cycles. The four segments were coded as I, II, III, and IV, each of length 250 ms which has been considered short enough as not to satisfy the assumption of non-stationarity, and long enough to meet the threshold of the higher-order statistical variances. The four coded segments ascribe to the following often occurring scenario; (I) Segment I, 0–250 ms; Predominantly maternal QRS-complex (no fetal QRS-complex present), (II) Segment II, 251 –500 ms; The first fetal heartbeat with maternal contribution, (III) Segment III, 501 ms – 750 ms; QRS-free ECG, and (IV) Segment IV, 751 – 1000 ms; The second fetal heartbeat with maternal contribution.

Fig. 4 (a), (b), (c), and (d) each depicts ECG signals (upper panel) and their third-order cumulants (lower panel) for fetal scalp ECG (550 ms), maternal chest ECG (900 ms), and two different and randomly picked transabdominally-measured maternal ECGs (1000 ms each). The subject is at 40 weeks gestation after the water has been broken hence facilitating fetal scalp measurements. The maternal cardiac cycle begins 50 ms before the R-wave and ends 50 ms before the next R-wave.

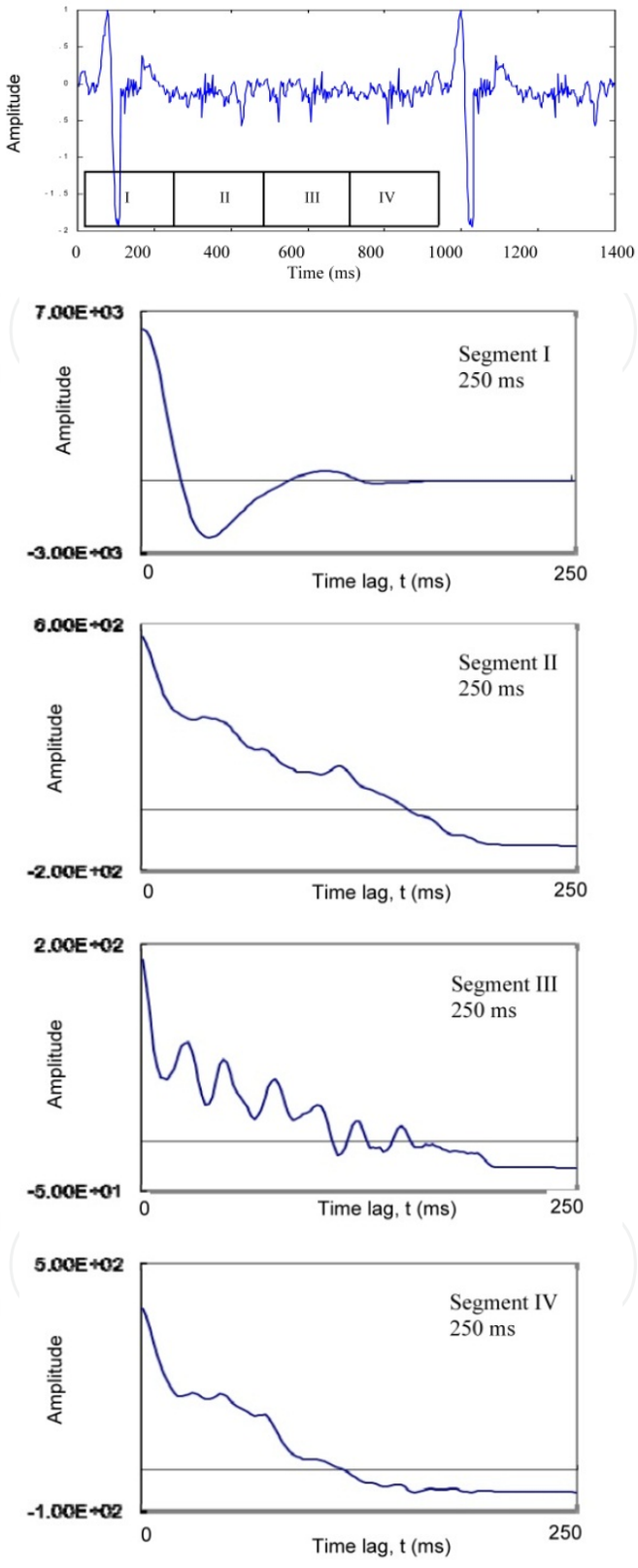

Figure 2. (a). Maternal transabdominal cardiac cycle (1000 ms) divided into four segments. The maternal cardiac cycle begins 50 ms before the R-wave and ends 50 ms before the next R-wave. The subject is at the first stage of labour (40 weeks gestation). (b). Typical examples of the second-order cumulants computed using the segments I, II, III, and IV shown in 2 (a) of maternal transabdominal ECG.

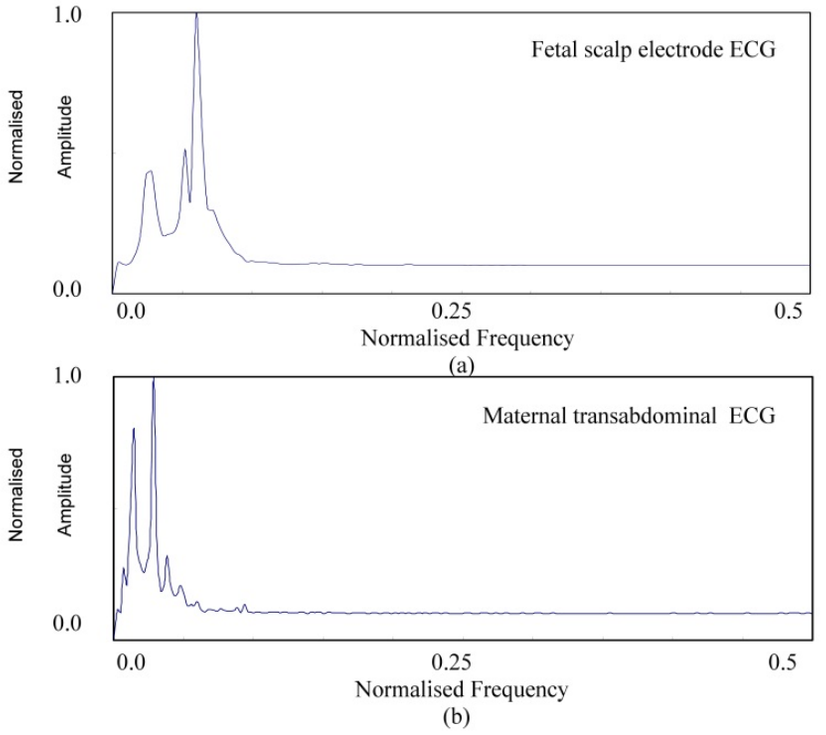

Figure 3. The power spectrum using the FFT method for (a) fetal scalp electrode ECG (data length 500 ms), and (b) maternal transabdominal ECG signal (data length 1000 ms). The maternal cardiac cycle begins 50 ms before the R-wave and ends 50 ms before the next R-wave. The subject is at the first stage of labour (40 weeks gestation).

A quick glance at the similarities of the four cumulant patterns in Fig. 4 (a), (b), (c) and (d), gives a little hope of successful detection of the fetal presence in the maternal cardiac cycle. To complicate the matter further, the two transabdominal cumulants in Fig. 4 (c) and (d) look dissimilar even though both contain two fetal QRS-complexes. However, the best way to distinguish between those patterns is to slice them and look for discriminant features.

Fig. 5 shows the third-order cumulants and their diagonal (l.h.s.) and wall (r.h.s.) slices of one transabdominal cardiac cycle which is segmented into four segments of 250 ms each for (I) predominantly maternal QRS, (II) the first fetal heartbeat with maternal contribution, (III) QRS-free ECG, and (IV) the second fetal heartbeat with maternal contribution. The diagonal and wall TOC slices of the maternal segment (I) are easily distinguished from the diagonal and wall TOC slices of segments (II), (III), and (IV). Furthermore, the diagonal and wall TOC slices of fetal QRS segments (II) and (IV) are distinguishable from the diagonal and wall TOC slices of the QRS-free ECG segment (III) in that there is a distinguishable and well-formed peak at the origin in both diagonal and wall TOC slices. The peak of the QRS-free ECG segment is much narrower and more related to motion artefact than a signal.

Note that having computed the three-dimensional TOCs, either the diagonal or the wall slice could be used in the detection / classification process. Therefore, computing the full multi-dimensional TOC and then extracting individual slices is an unnecessary waste of the CPU time. So, why not compute any arbitrary 1-d slice directly without firstly having to

compute the two-dimensional TOC and secondly extract the 1-d slice? The TOC-diagonal and the TOC-wall slices are straightforward to compute directly, by freezing one of the two cumulant lags and changing the other one. However, computing any other arbitrary slice requires the development of an auxiliary algorithm (Zgallai, 2007). It has been found that performing direct computations of the 1-d TOC slices instead of computing the 2-d TOC firstly and secondly extracting individual 1-d slices results in saving of more than 99% of the CPU time.

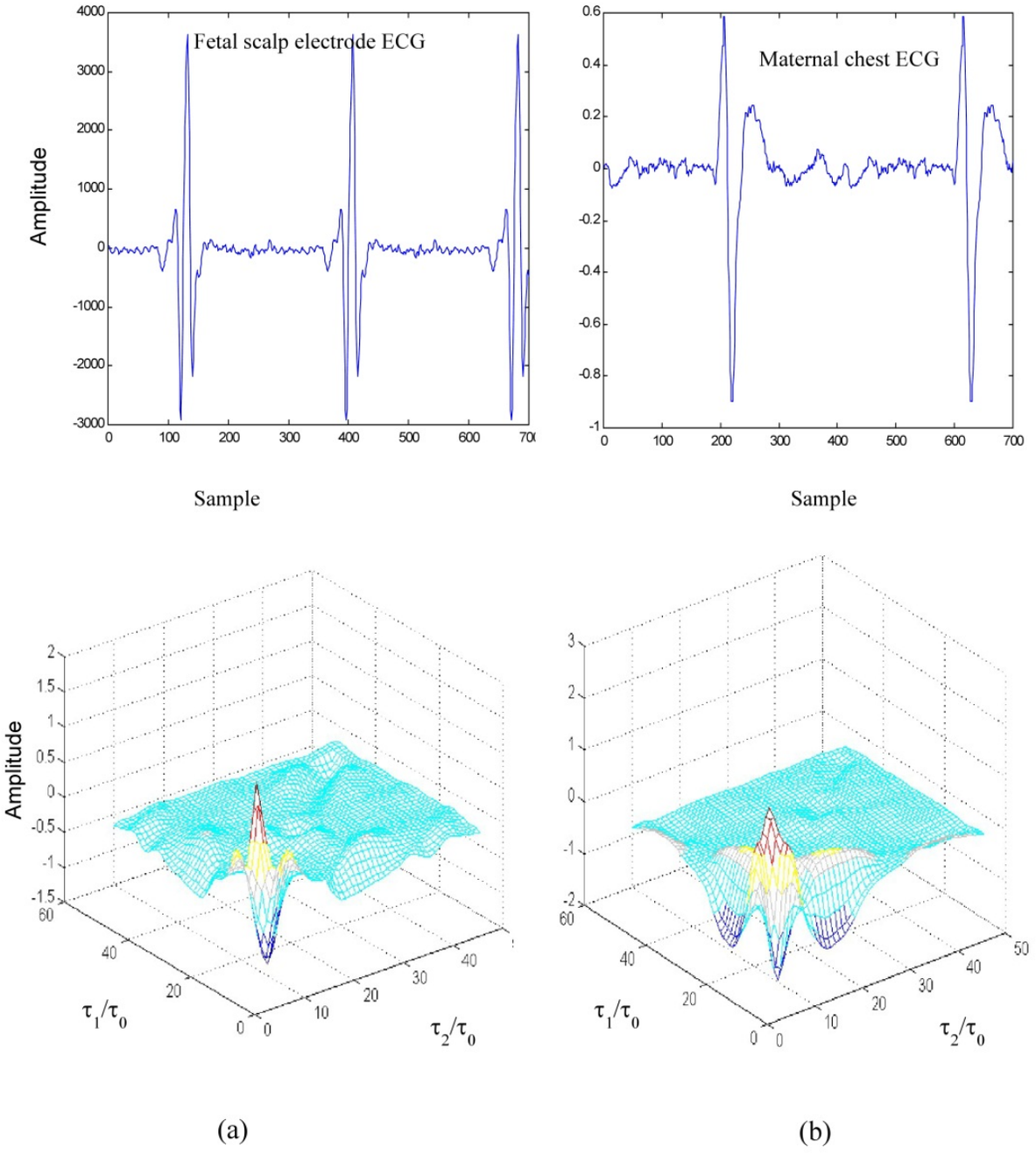

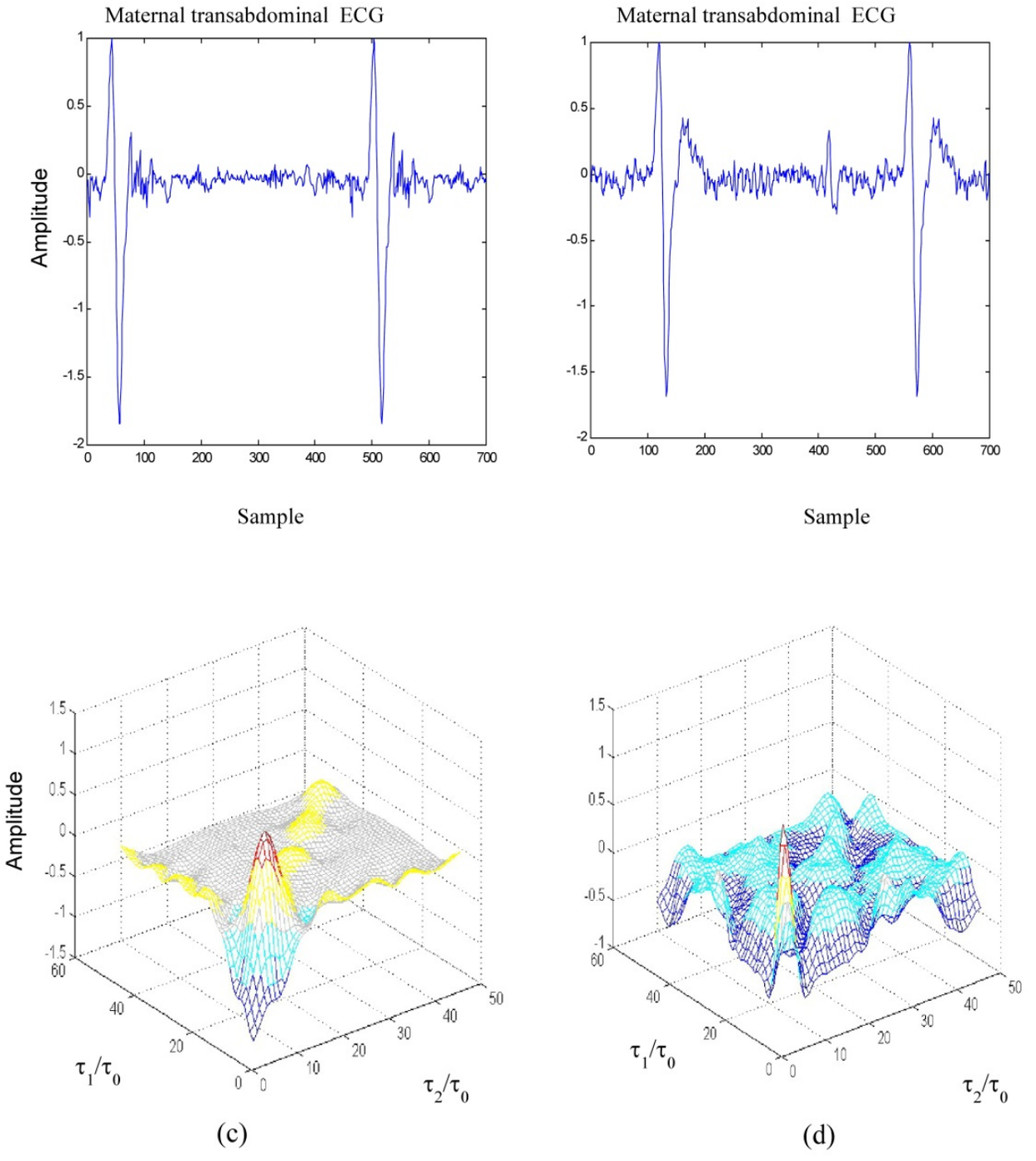

Figure 4. ECG signals (upper panel) and their third-order cumulants (lower panel) for (a) fetal cardiac cycle using fetal scalp electrode (data length 550 ms), (b) maternal chest cardiac cycle using one surface electrode and a reference electrode (data length 900 ms), (c) and (d) are two maternal transabdominal cardiac cycles measured using twin surface electrodes (data length 1000 ms each). The maternal cardiac cycle begins 50 ms before the R-wave and ends 50 ms before the next R-wave. The subject is at the first stage of labour, 40 weeks.

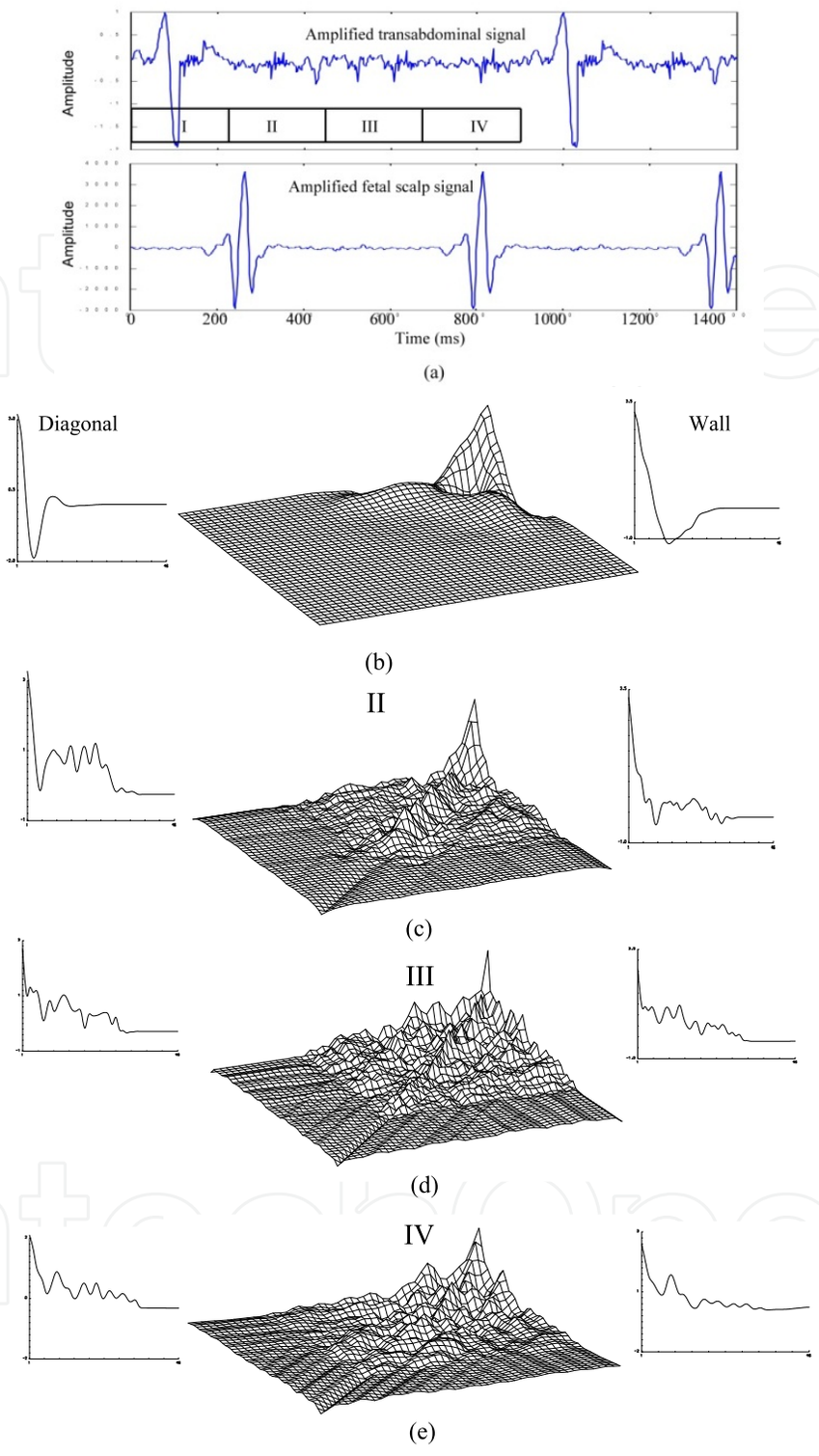

Figure 5. (a) Maternal transabdominal ECG signal (upper panel) and the synchronised fetal ECG signal measured using fetal scalp electrode (lower panel). (b), (c), (d) and (e) are the third-order cumulants and their diagonal (l.h.s.) and wall (r.h.s.) slices for segments I, II, III, and IV, respectively, each segment is 250 ms. Segment I: pre-dominantly maternal QRS-complex, segment II, the first fetal heartbeat with maternal contribution, segment III: QRS-free ECG, and segment IV: the second fetal heartbeat with maternal contribution. The maternal cardiac cycle begins 50 ms before the R-wave and ends 50 ms before the next R-wave.

Fig. 6 shows four selected slices of the third-order cumulants computed using one cardiac cycle for each of the following; (a) and (b) an adult male and female chest, respectively, (c) maternal transabdominal, and (d) fetal scalp electrode ECG signal.

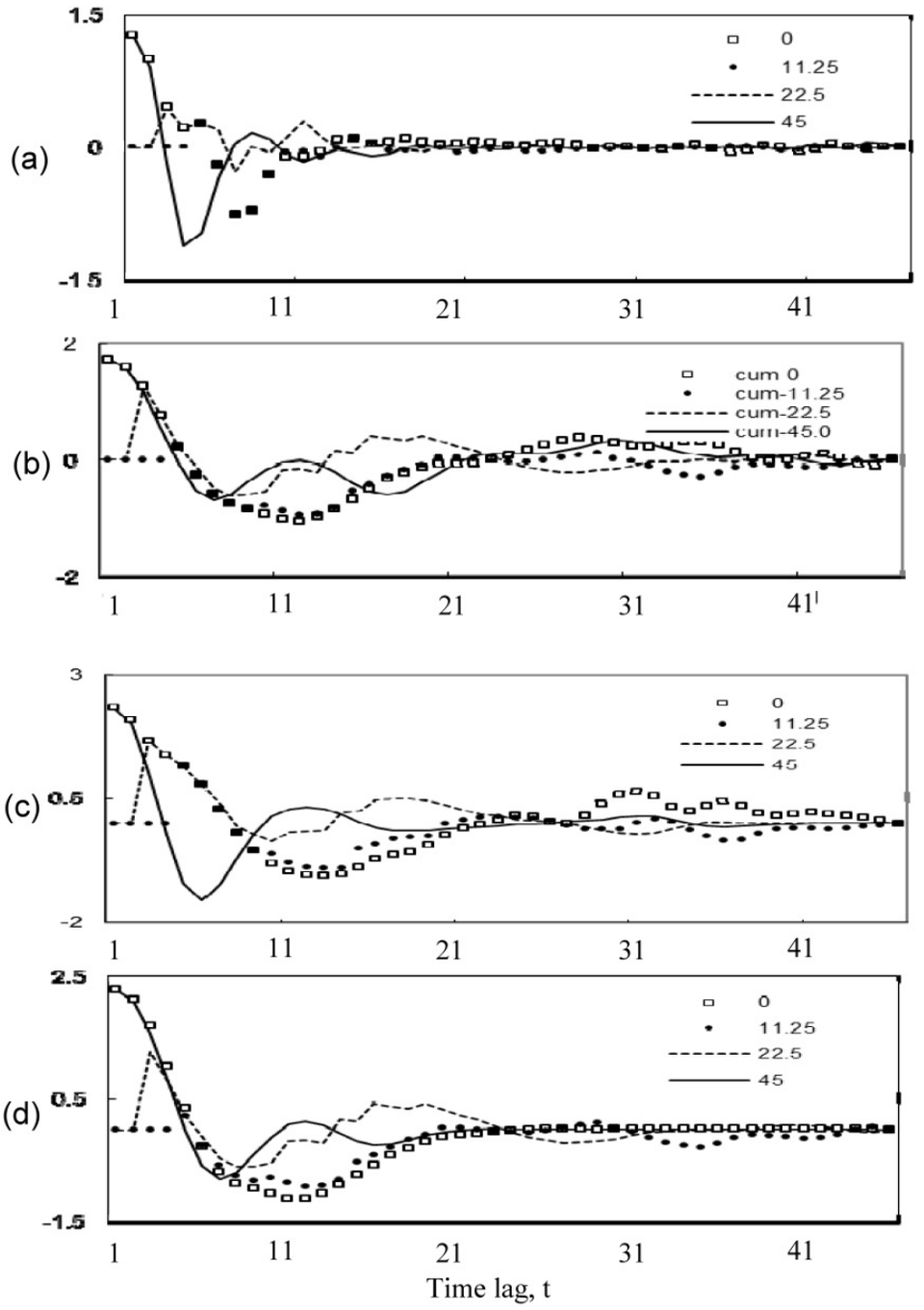

Figure 6. Third order cumulant slices at 0^o (wall), 11.25^o , 22.50^o, and 45^o (diagonal) for (a) male chest cardiac cycle using one surface electrode (data length 1180 ms), (b) maternal chest cardiac cycle using one surface electrode (data length 900 ms), (c) maternal transabdominal cardiac cycle using twin surface electrodes (data length 1000 ms), and (d) fetal cardiac cycle using fetal scalp electrode (data length 550 ms). The maternal cardiac cycle begins 50 ms before the R-wave and ends 50 ms before the next R-wave. The female subject is at the first stage of labour, 40 weeks gestation.

4.2. The bispectrum, contour maps and slices for cardiac cycles

Fig. 7 shows the bispectrum magnitudes (left panel) and the corresponding contours (right panel) using one cardiac cycle for; (a) fetal scalp electrode ECG, (b) maternal chest ECG, and (c) maternal transabdominal ECG signal. Before attempting to assess any advantages of the ECG bispectrum over and above the power spectrum one should regress,

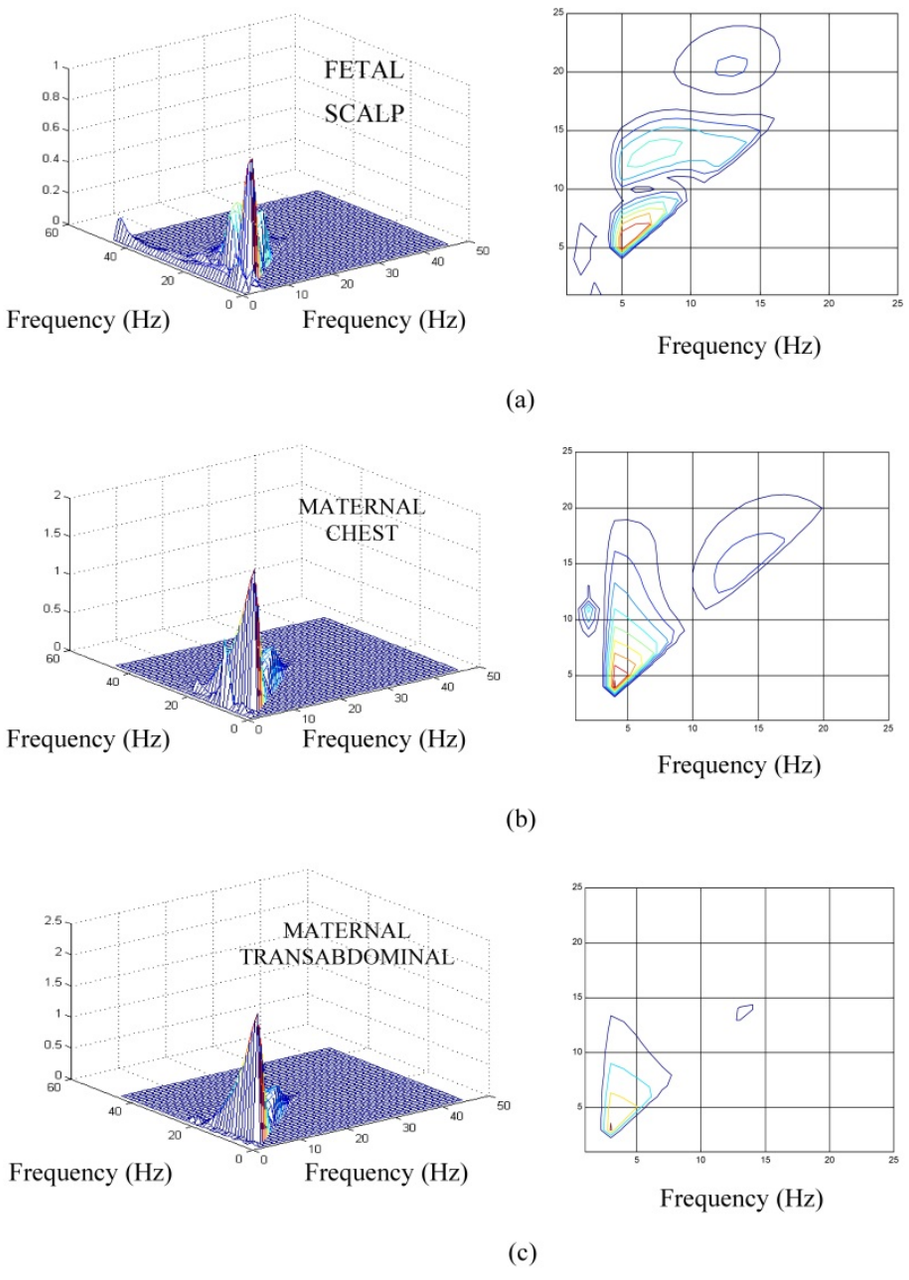

Figure 7. The bispectrum magnitude (left panel) and contour map (right panel) for (a) a fetal cardiac cycle using fetal scalp electrode (data length 550 ms), (b) a maternal chest cardiac cycle (data length 1000 ms), and (c) a maternal transabdominal cardiac cycle (data length 1000 ms). The maternal cardiac cycle begins 50 ms before the R-wave and ends 50 ms before the next R-wave. The subject is at the first stage of labour, 40 weeks gestation. The direct method is used to calculate the bispectrum.

for a moment, to view the power spectrum and locate the frequency ranges for adult and fetal QRS-complexes. The power spectrum of appropriately sampled ECG showed the QRS-complex principal peak in the frequency range from 15 Hz to 20 Hz, and 25 Hz to 40 Hz, for the maternal chest ECG and fetal scalp electrode ECG, respectively. The power spectrum has limitations as an estimator in terms of resolution, variance, and clarity of the spectrum to be able to produce clear and distinguishable peaks for the P-waves. An alternative spectrum estimator was used instead, namely, the multiple signal classification (MUSIC) pseudo-spectrum. The MUSIC-based pseudo-spectrum also showed that the principal peaks for the p-waves occupy a range from 5 Hz to 8 Hz for adults. The principal peaks for the P-waves of the fetal scalp electrode ECG occupy a range from 8 Hz to 10 Hz. The same MUSIC-based spectral estimators have revealed high local energy peaks around 5 Hz due to motion artefact (Zgallai, et al., 1997).

It is clearly seen in Fig. 7 that all significant twin-frequency peaks occur at frequencies lower than the p-wave and QRS-complex frequencies. It is very difficult to observe any p-wave or QRS-complex frequencies. The only thing that could be construed from these results is that the combined effect of the low temporal resolution resulting from using the whole cardiac cycle and the low spectral resolution inherent in the bispectrum formation, the QRS-complex twin peaks which should occur at frequency ranges from (15 Hz, 15 Hz) to (20 Hz,20 Hz) for adults and from (25 Hz,25 Hz) to (40 Hz,40 Hz) for fetal scalp electrode ECG are completely masked and cannot be found even at –30 dB normalised to any significant low frequency peak. Instead, only low frequencies predominate (Zgallai, 2012 b).

Fig. 8 shows the bispectra of fetal scalp electrode and maternal chest ECG signals (left panel) and the corresponding contour maps (right panel). The maternal cardiac cycle begins 50 ms before the R-wave and ends 50 ms before the next R-wave. The subject is at the first stage of labour, 40 weeks gestation. The bispectrum is calculated using the direct method which involves calculating a two-dimensional Fourier transform. Ten Hanning windows is used in calculating the bispectrum which are averaged for smoothing. The bispectral peaks of the fetal scalp electrode and maternal chest QRS-complexes exist at (40 Hz,40 Hz) and (13 Hz,13 Hz), respectively. However, they are shifted, shallow and inconclusive even though they are centred near the right frequency pairs, (30 Hz,30 Hz) for the fetal scalp electrode and (17 Hz,17 Hz) for the maternal chest ECG.

The temporal resolution could be improved by applying appropriate segmentations to the QRS-complexes. Instead of taking one cardiac cycle for an adult, which is on average 1000 ms, the 250 ms QRS-complex segment which is centred on the R-wave and runs 125 ms in opposite directions is considered. This also applies to the fetal scalp electrode ECG signal but with a reduced QRS-complex length of typically 60 ms.

Fig. 9 (top) depicts bispectral slices of the fetal QRS-complex which shows the correct position of a spectral peak at 30 Hz but only on the diagonal slice. Fig. 9 (middle and bottom) show maternal chest and transabdominal QRS-complex **bispectrum** slices. The maternal chest and abdomen both exhibit spectral frequencies of 17 Hz and 15 Hz, respectively, but only on the diagonal slice. Considerable improvement has resulted due to

improving the temporal resolution prior to the bispectral calculations for both fetal and maternal chest segmented QRS-complexes. However, looking at the maternal chest and transabdominal bispectral diagonal slices, lowering of the QRS peak frequency from 17 Hz to 15 Hz is observed.

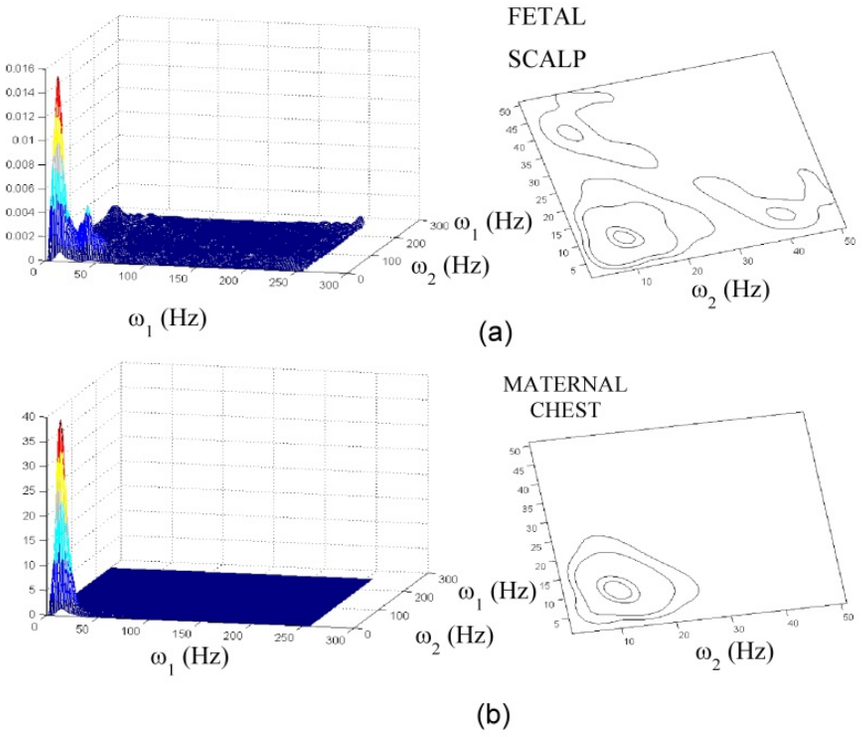

Figure 8. The bispectra of (a) a fetal scalp and (b) a maternal chest ECG signal (left panel) and the corresponding contour maps (right panel). The maternal cardiac cycle begins 50 ms before the R-wave and ends 50 ms before the next R-wave. The subject is at the first stage of labour, 40 weeks gestation. The bispectrum is calculated using the direct method. A Hanning window is used to calculate the bispectrum which is averaged for smoothing.

A possible cause of this shifting in the QRS-complex frequency peak is the susceptibility and lack of predictability of the bispectral representation of highly-complex multi-frequency signals. During labour contractions, the presence of very strong deterministic and chaotic signals emanating from the uterus, and the accompanying motion artefacts result in highly dimensional transabdominal signals (Rizk et al., 2000) is shown. Consequently it is very difficult to isolate with integrity the maternal and fetal QRS- complex spectral peaks without first resorting to super-resolution algorithms using eigenvector-based projections (Zgallai, 2007).

4.3. Non-linearity of ECG signals

The non-linearity in the ECG signal can be detected using the bicoherence squared. Fig. 10 depicts the bicoherence squared and their corresponding contour maps using one cardiac cycle for a fetal scalp electrode, maternal chest, and maternal transabdominal ECG. The bicoherence squared has peaks at the frequency pairs of (6 Hz,15 Hz) and (14 Hz,14 Hz) for the fetal scalp cardiac cycle, (15 Hz,15 Hz) for the maternal chest cardiac cycle, and (7.5

Hz,7.5 Hz) for the maternal transabdominal cardiac cycle. These bicoherence peaks support non-linearity.

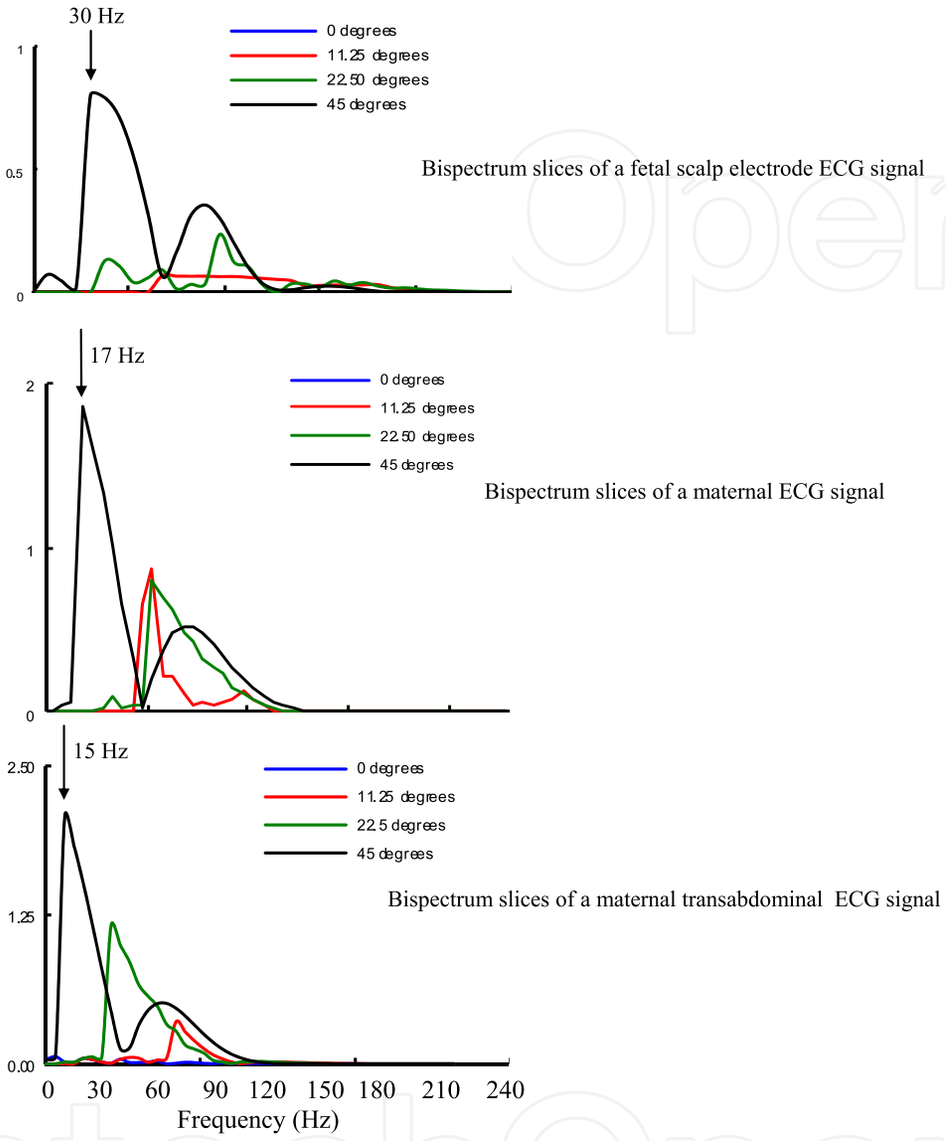

Figure 9. Bispectrum slices at 0° (wall), 11.25° , 22.50°, and 45° (diagonal) for 250 ms segments of; fetal cardiac cycle using fetal scalp electrode (upper panel), maternal chest cardiac cycle (middle panel), and maternal transabdominal cardiac cycle (lower panel). The maternal cardiac cycle begins 50 ms before the R-wave and ends 50 ms before the next R-wave. The subject is at the first stage of labour, 40 weeks gestation.

4.4. Proximity of the maternal and fetal QRS- complexes

There is a general consensus that individual cardiac cycles are locally stationary. This was substantiated (Zgallai, 2007) by Hinich test (Hinich, 1982). However, when applying a highly dimensional signal such as the transabdominal ECG that have several individual non-linear and deterministic signals overlapping both in the time and frequency domains, all coexisting in a cocktail of noise and motion artefact, it is prudent to re-examine the

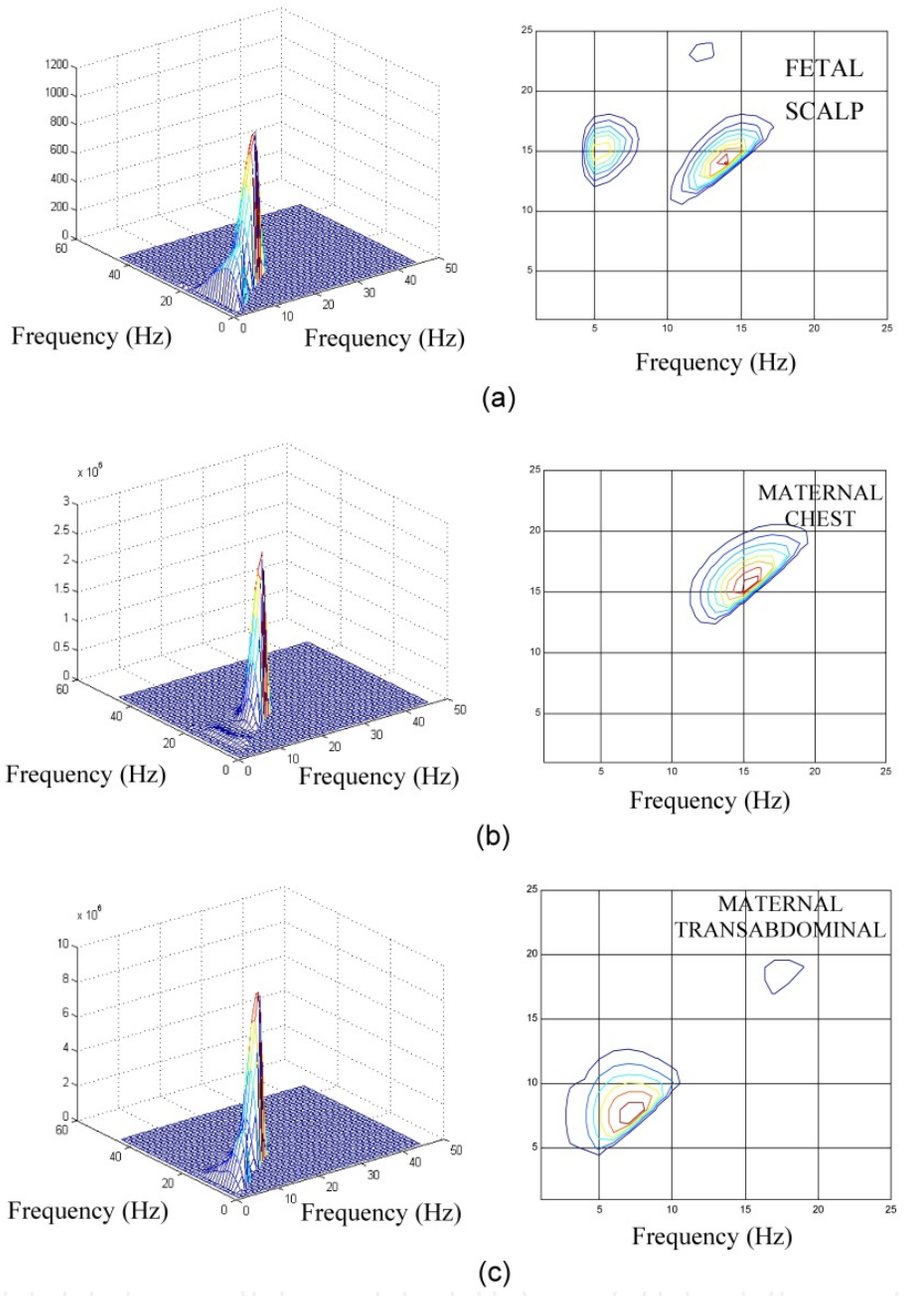

Figure 10. The bicoherence squared (left panel) and contour map (right panel) for (a) a fetal cardiac cycle using fetal scalp electrode (data length 550 ms), (b) a maternal chest cardiac cycle (data length 1000 ms), and (c) a maternal transabdominal cardiac cycle (data length 1000 ms). The maternal cardiac cycle begins 50 ms before the R-wave and ends 50 ms before the next R-wave. The subject is at the first stage of labour, 40 weeks gestation. The bispectrum is calculated using the direct method. A Hanning window is used to calculate the bispectrum which is averaged for smoothing.

validity of the stationarity assumption in relation to such signals. It is only natural to expect that the proximity of two non-linear signals such as the maternal and fetal QRS-complexes would result in non-linear (quadratic and higher-order) coupling and this in turn would invoke non-stationarity. The above is demonstrated to be true by inspecting the bispectral OT region shown in Fig. 11. The maternal cardiac cycle in Fig. 11 begins 50 ms

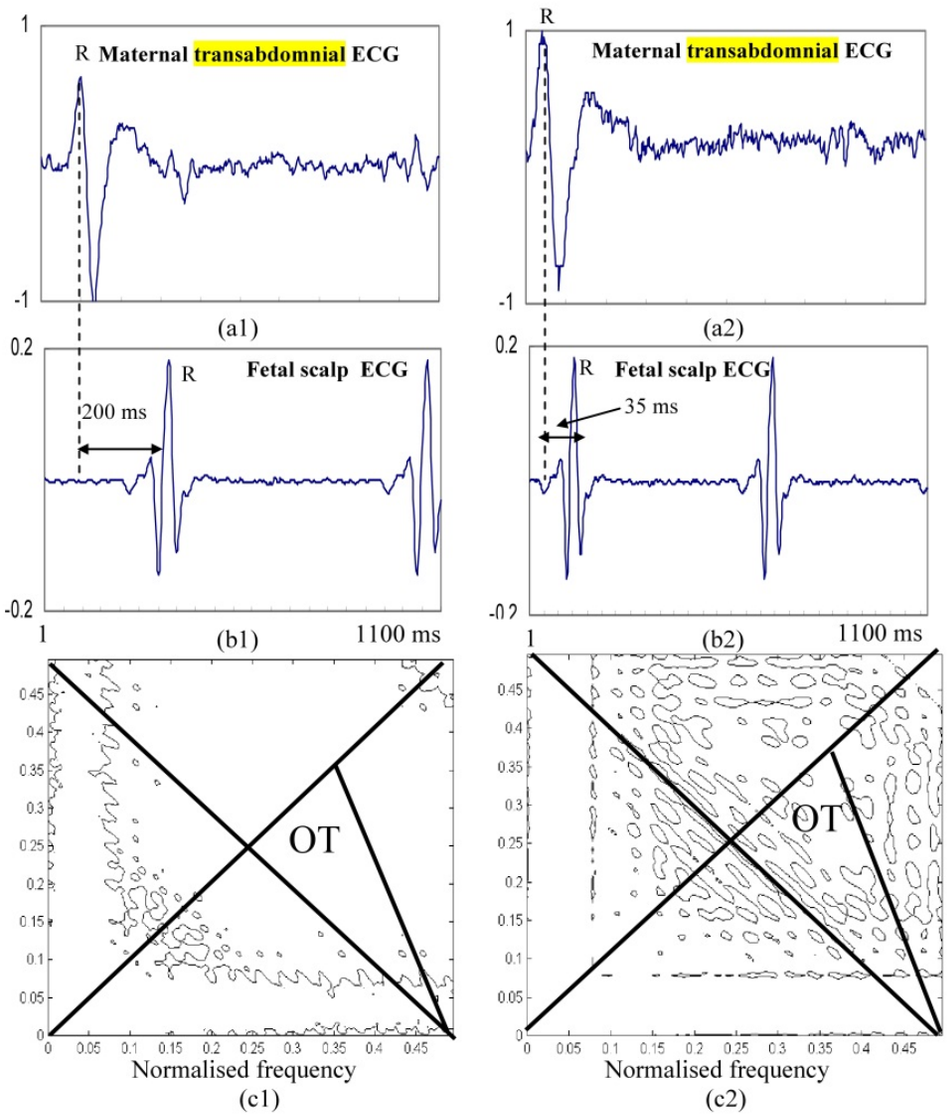

Figure 11. (a1), (a2) Two typical examples of maternal transabdominal cardiac cycles, (b1) and (b2) are the corresponding fetal ECG signals using fetal scalp electrode. The first fetal QRS-complex in (b1) is separated from the maternal QRS-complex in (a1) by 200 ms. The first fetal QRS-complex in (b2) is separated from the maternal QRS-complex in (a2) by 35 ms. The corresponding bispectrum contour maps at a level of -30 dB for the two cycles in (a1) and (a2) are shown in (c1) and (c2), respectively. The R-wave of the first fetal QRS-complex in (b1) is separated from the R-wave of the maternal QRS-complex in (a1) by 200 ms. The corresponding bispectrum in (c1) does not show extra activity in the OT region. The R-wave of the first fetal QRS-complex in (b2) is separated from the R-wave of the maternal QRS-complex in (a2) by 35 ms. The corresponding bispectrum in (c2) shows extra activities in the OT region due to non-linear coupling between the mother and the baby.

before the R-wave and ends 50 ms before the next R-wave. The subject is at the first stage of labour, 40 weeks gestation. Fetal cardiac cycle data length is 550 ms, and transabdominal ECG cardiac cycle data length is 1000 ms. Two typical transabdominally measured maternal ECG cycles, ((a1), (a2)), and two synchronised fetal scalp ECG cycles ((b1), (b2)) are shown. The lower parts of the Figure, (c1) and (c2), consist of the corresponding maternal bispectral contour maps at a level of -30 dB. The two R-waves of the maternal and fetal QRS-

complexes in (a1) and (b1), respectively, are separated by 200 ms. The resultant bispectrum in (c1) does not support the OT region. However, the situation is totally different when the two R-waves are as close as 35 ms as shown in Fig. 11 (a2) and (b2). Now the OT region of the bispectrum in (c2) is fully occupied and non-stationary. This means conventional signal processing techniques cannot be used to separate the maternal and fetal QRS-complexes. This problem has been adequately solved by linearising (at least removing quadratic coupling) the transabdominal signal before attempting to separate individual QRS-complexes.

4.5. Cumulants and bispectra of noise components

The MIT/BIH databases (MIT/BIH, 1997) have recordings of the three main types of noise in ECG signals, namely, (a) baseline wander, (b) electro-myographic (EMG) noise, and (c) motion artefact. The following statistics help in the processing stages of the fetal heartbeat detection. When using super-resolution techniques requirement for Gaussian and non-Gaussian extraction and suppression is eliminated except for the conventional removal of baseline wander which is embedded in all data acquisition systems (baby monitors).

a. Baseline Wander noise

Fig. 12 depicts second- and third-order statistics of a baseline wander noise segment of 10,000 samples (approximately 30 sec) extracted from the MIT/BIH databases. Both the bispectrum and the bicoherence squared show high peaks at low frequencies (< 5 Hz). This means that the effect of the baseline wander noise on both maternal and fetal QRS-complexes at 15 Hz and 30 Hz, respectively, is not significant. It is prudent to eliminate such noise in the pre-processing stage. One conventional method of eliminating baseline wander employs a high-pass filter such as Butterworth high-pass filter of order 5, cut-off frequency of 1 Hz, a transition period of 1 Hz, a minimum ripple of –50 dB outside the main frequency lobe.

b. Electromyographic noise

Fig. 13 shows some statistics of an electromyographic (EMG) noise segment of 10,000 samples extracted from the MIT/BIH databases. The noticeable feature is that the bispectrum is confined to low frequencies less than (10 Hz,10 Hz). This means that it will not interfere with the isolation of the adult QRS-complex bispectrum peak which occupies frequencies between (15 Hz,15 Hz) and (20 Hz,20 Hz), provided that an appropriate super-resolution technique is employed. But the bicoherence squared of the EMG noise is spread over a wide band of frequencies, up to (120 Hz, 120 Hz). The carpet effect of the non-linearity attributed to the EMG noise will be eliminated by linearising the transabdominal signal prior to fetal QRS-complex detection in the third-order statistical domain. Under broad signal and noise conditions, linearisation of the transabdominal ECG signal not only removes to a great extent the signal non-linearity, but also partially eliminates other types of non-linearity due to noise.

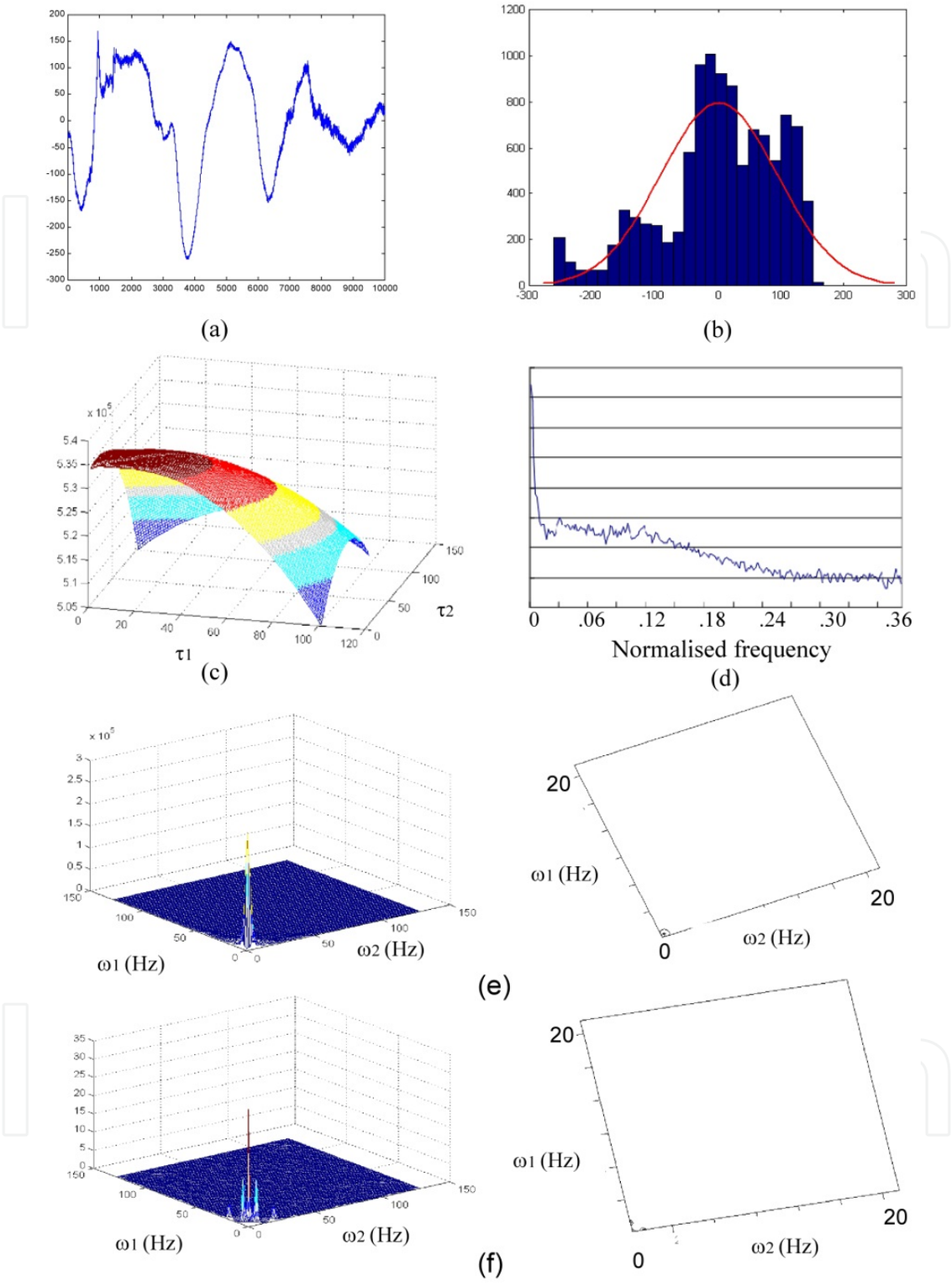

Figure 12. Characterisation of 10,000 samples of baseline wander noise extracted from the MIT/BIH database and sampled at 360 samples per second. (a) time series, (b) its histogram showing non-Gaussian pdf, (c) third-order cumulants, (d) power spectrum using the averaged periodogram method, (e) the bispectrum (l.h.s.) calculated using the direct method with contour maps (r.h.s.) and (f) the bicoherence squared (l.h.s.) with contour maps (r.h.s.).

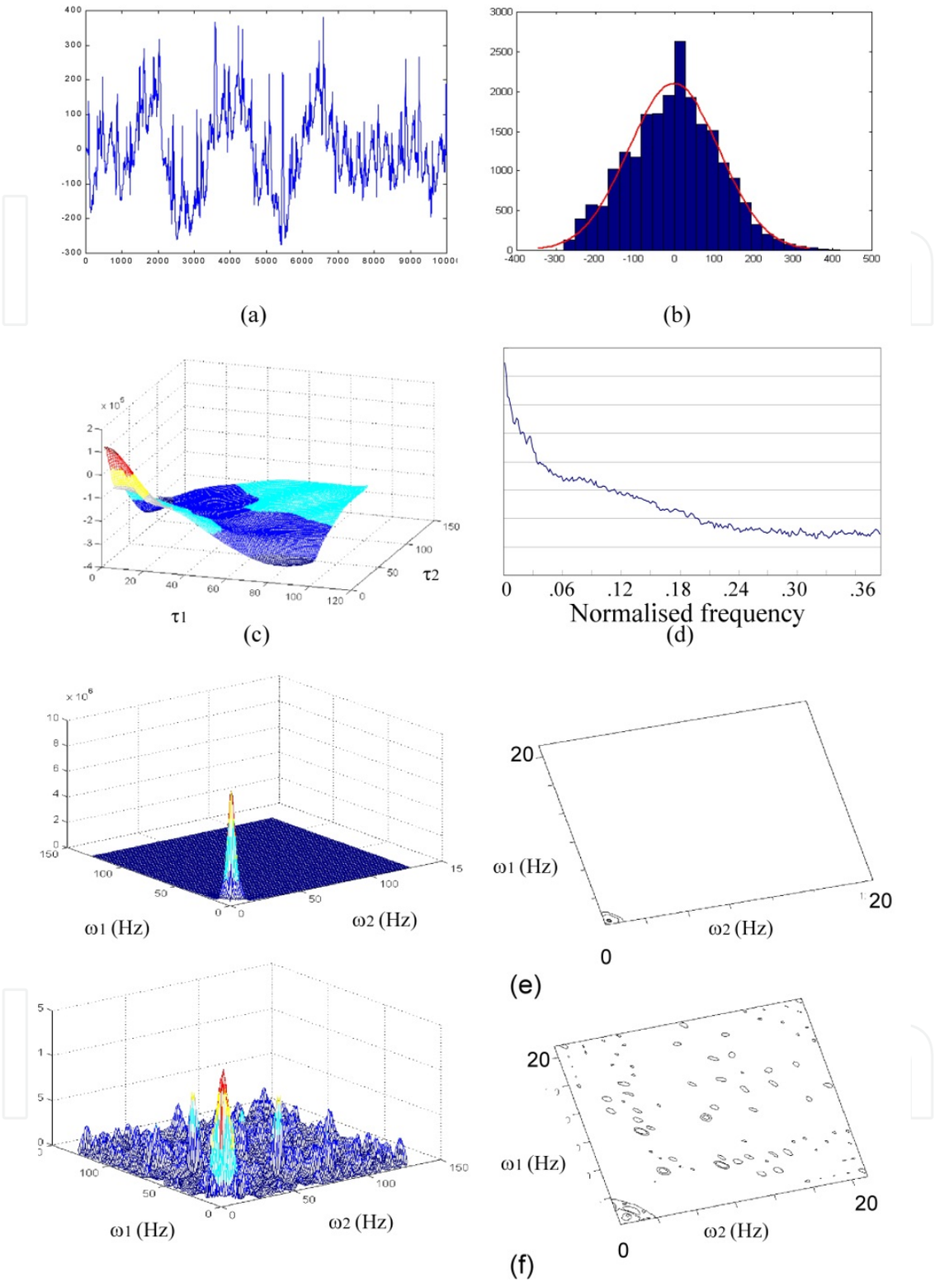

Figure 13. Characterisation of 10,000 samples of electromyographic noise extracted from the MIT/BIH database and sampled at 360 samples per second. (a) time series, (b) its histogram, (c) third-order cumulants, (d) power spectrum using the averaged periodogram method, (e) the bispectrum (l.h.s.) calculated using the direct method with contour maps (r.h.s.) and (f) the bicoherence squared (l.h.s.) with contour maps (r.h.s.).

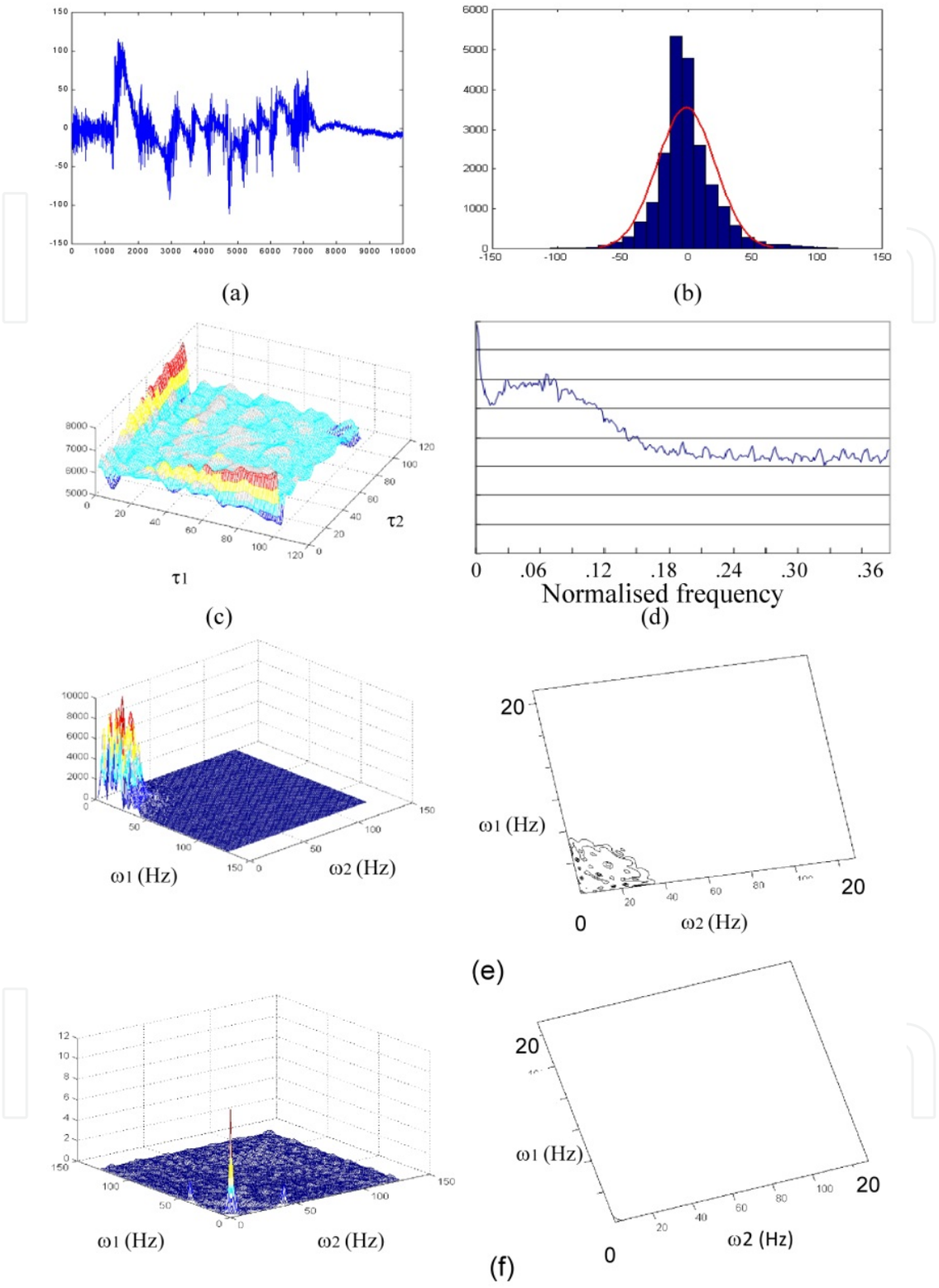

Figure 14. Characterisation of 10,000 samples of motion artefact noise extracted from the MIT/BIH database and sampled at 360 samples per second. (a) time series, (b) its histogram, (c) third-order cumulants, (d) power spectrum using the averaged periodogram method, (e) the bispectrum (l.h.s.) calculated using the direct method with contour maps (r.h.s.) and (f) the bicoherence squared (l.h.s.) with contour maps (r.h.s.).

c. Motion artefact noise

Fig. 14 depicts second- and third-order statistics of a motion artefact noise segment of 10,000 samples extracted from the MIT/BIH databases. The bispectrum has many frequencies in the triangle region of (0 Hz,0 Hz), (0 Hz,35 Hz) and (35 Hz,0 Hz). These bispectral frequencies of motion artefact would be overlapping with those of the maternal and fetal QRS-complexes, albeit at around –20 dB level. However, the level of noise at the QRS-complex spectra is comparatively small and the effect of motion artefact on the detection of QRS-complexes is not noticeable. Fig. 14 (f) reveals that the bicoherence squared is rather confined to very low frequencies. As mentioned above, linearisation plays a definitive role.

5. Discussion and conclusions

The objective of this chapter is to introduce the subject of higher-order statistics (HOS) and its applications to the non-linear / non-Gaussian ECG signals to pave the way for employing HOS-based techniques as the solution to the formidable problem of transabdominal fetal heartbeat detection during labour. High detection rates can be accomplished by invoking the HOS-based techniques, namely, the third-order cumulant template matching and the bispectral contours template matching and which utilises a set of different levels of bispectral contours.

The key question that was attempted is why do HOS-based techniques yield the highest possible Fetal Heart Rate FHR? The reasons behind achieving high FHRs when using the HOS-based well-refined techniques are; (1) Under broad signal and noise conditions, higher-order cumulants and their spectra become high signal-to-noise ratio domains where detection, parametric estimation and signal classification can be performed. (2) The Gaussian noise diminishes in the HOS domains if the data length is adequate. For ECG signals, a minimum length of 1 sec is sufficiently long to suppress Gaussian noise and maintain a low level of HOS variances in the HOS domains, whilst not sufficiently long to violate Hinich's criterion for local stationarity. (3) In the third-order domain all sources of noise with symmetric probability density functions (pdfs), e.g., Gaussian and uniform, will vanish. The ECG signals are retained because they have non-symmetric distributions. This implies that it is more than adequate to utilise only the TOCs and their bispectra. There is no need to seek higher-than-third-order statistics as implicated in all the Independent Component Analysis (ICA) applications to FHR detection. (4) The maternal and fetal QRS-bispectral contours, which are used as the discriminant patterns in the identification and classification, only overlap with the bispectra of the baseline wander and that of the EMG at very low levels (around –20 dB normalised to the peak of the maternal QRS-complex bispectrum). Therefore, it is comparatively easy to detect and classify QRS-complexes in ECG signals utilising either the TOC or the BIC template matching techniques.

5.1. Direct computations of individual 1-d TOC slices

It is also shown that, having computed the two-dimensional TOC, either the diagonal or the wall slice or a combination of the diagonal and wall slices is used in the detection /

classification process. Therefore, computing the full multi-dimensional TOC and then extracting individual slices is an unnecessary waste of the CPU time. So, why not compute any arbitrary 1-d slice directly without firstly having to compute the two-dimensional TOC and secondly extract the 1-d slice? The TOC-diagonal and the TOC-wall slices are straightforward to compute directly, by freezing one of the two cumulant lags and changing the other one. However, to compute any other arbitrary slice requires the development of an auxiliary algorithm. It has been found that performing direct computations of the 1-d TOC slices instead of computing the 2-d TOC firstly, and secondly extracting individual 1-d slices results in saving of more than 99% of the CPU time. The same applies to the 2–d bispectrum. However, it has to be borne in mind that it is the matching of the horizontal bispectral contours that is used in the Bispectral Contour (BIC) template matching technique instead of the 1-d polar bispectral slices. Because in order to use the 1-d polar bispectrum slices effectively one needs to use a minimum of 24 polar slices so as not to miss the capturing of rapid changes or null features in the bispectrum that could be used as discriminant patterns. Whereas for BIC contours the number of discriminant horizontal slices required for detection / classification does not exceed 10.

5.2. Bispectral features of QRS-complexes

The power spectrum of appropriately sampled ECG showed the QRS-complex principal peak in the frequency range from 15 Hz to 20 Hz, and 25 Hz to 40 Hz, for the maternal chest ECG and fetal scalp electrode ECG, respectively. Unfortunately, the power spectrum has limitations as an estimator in terms of resolution, variance, and clarity of the spectrum to be able to produce clear and distinguishable peaks for the P-waves. Therefore, an alternative spectrum estimator was used instead, namely, the multiple signal classification (MUSIC) pseudo-spectrum. The MUSIC-based pseudo-spectrum showed that the principal peaks for the p-waves occupy a range from 5 Hz to 8 Hz for adults. The principal peaks for the P-waves of the fetal scalp electrode ECG occupy a range from 8 Hz to 10 Hz. The same MUSIC-based spectral estimators have revealed high local energy peaks around 5 Hz due to motion artefact (Zgallai et al., 1997).

As with cumulants, their bispectra were computed for the above mentioned ECG data samples and segmentations using the direct method which involves calculating a two-dimensional Fourier transform. The following bispectral peaks have been observed only on the bispectral diagonal slice at the following frequency pairs;

a. (17 Hz,17 Hz) and (15 Hz,15 Hz) for the maternal chest and the transabdominal ECGs, respectively. So, there is a shift in the bispectral peak from 17 Hz to 15 Hz in the transabdominal ECG.
b. (30 Hz,30 Hz) and less prominently at (20 Hz,20 Hz) for the fetal scalp electrode ECG.

5.3. Quadratic coupling in transabdominally measured ECG signals

It has been found in maternal transabdominal ECG signals that close proximity of the maternal and fetal QRS-complexes initiates additional quadratic and higher-order non-

linearities that could be due to higher-order coupling of the maternal and fetal own harmonics and the concomitant mixing of the ECG signals and the non-linear uterine contraction interference signal. This so called coupling between maternal and fetal ECGs (Rizk et al., 2001) is manifested in a newly formed bicoherence squared peak(s) which did not exist in either of the isolated maternal bicoherence squared or the isolated fetal bicoherence squared computed from their respective ECG signals. The non-linear second- or third-order Volterra structure has been used (Rizk et al., 2001) to quantify the effect of this coupling, in part. The rest of the quantification process is carried out using the bicoherence squared.

It is worth mentioning that, depending on the bispectrum estimation method employed, the techniques for the detection and quantification of quadratic phase coupling are divided into two categories: the conventional and the parametric. The conventional techniques are based on the bicoherence spectrum and they are better qualifiers of the phase coupling (Kim and Powers, 1978; Kim and Powers, 1995). However, their resolution is limited by the uncertainty principle of the Fourier transform. On the other hand, the parametric techniques are based on the auto-regressive (AR) modelling of the third-order cumulants. Although the parametric AR methods are not good quantifiers, they possess a high resolution capability, much higher than the frequency resolution of the conventional methods (Nikias and Raghuveer, 1987; Raghuveer and Nikias, 1986). The so called coupling results in non-stationarity in the transabdominal ECG signal. This is evidenced by the filling of the bispectrum OT region which is used as a measure of non-stationarity in non-Gaussian signals.

5.4. Noise identification in male and non-pregnant female adults

For noise identification and characterisation in the third-order domain, the MIT/BIH databases were utilised (MIT/BIH 1997). Apart from Gaussian noise, there exist three types of non-Gaussian noise in ECG signals, namely, baseline wander, electromyographic (EMG), and motion artefact noise. 10,000 samples of each of these three types of noise are analysed. A brief summary of their third-order statistics is shown in Table 1.

	Baseline wander	Electromyographic	Motion artifact
Third-order cumulants	Support	Support	Support
Bispectrum	Frequency < 5 Hz	Frequency < 10 Hz	Frequency < 35 Hz
Bicoherence Squared	Frequency < 5 Hz	Frequency < 120 Hz	Frequency < 5 Hz

Table 1. Third-order statistics of three types of noise in ECG signals; baseline wander, electromyographic noise, and motion artefact.

The effect of the baseline wander noise on both the maternal and the fetal QRS-complexes at 15 Hz and 30 Hz, respectively, is not significant. Table 1 shows that only the bispectrum of

the motion artefact and the bicoherence squared of the EMG noise have frequencies that would potentially overlap with those of the QRS-complexes of the mother and the fetal, albeit at –20 dB level. The bicoherence squared of the EMG noise is spread over a wide band of frequencies, up to (120 Hz ,120 Hz). The carpet effect of the non-linearity attributed to the EMG noise will be significantly reduced by linearising the transabdominal signal prior to fetal QRS detection in the third-order statistical domain. Under broad signal and noise conditions, linearisation of the transabdominal ECG signals not only removes to a great extent the signal non-linearity, but also partially eliminates other types of non-linearity due to noise or non-linearity due to strong uterine contractions.

It could be deduced from Table 1 that there would be overlapping between the bispectral frequencies of motion artefact and those of the maternal and the fetal QRS-complexes, albeit at around –20 dB level. However, the level of noise at the QRS-complex spectra is comparatively small and by using QRS-complex tailor-made spectral windows, the effect of motion artefact on the detection of the QRS-complexes is not noticeable.

Author details

Walid A. Zgallai
Berkshire, UK
Dubai, UAE

6. References

Brillinger,D. R. (1965). "An Introduction to Polyspectra," *Annals of Mathematical Statistics*, vol. 36, pp. 1351-1374.

Brockett, P. L.; Hinich, M. J.; and Patterson, D. (1988). "Bispectral-Based Tests for the Detection of Gaussianity and Linearity in Time Series," Journal of the American Statistical Association, vol. 83, No. 403, pp. 657-664.

Friedlander, B. and Porat, P. (1988). "Performance analysis of MA parameter estimation algorithms based on higher-order moments," *Proceedings of IEEE Int Conf Acoustics, Speech and Signal Processing (ICASSP)*, pp. 2412-2415, NY, April.

Hinich, M. J. (1982). "Test for Gaussianity and linearity of a stationary time series," *Journal of time series analysis*, vol. 3, No. 3, pp. 169-176.

Kim, Y. and Powers, E. J. (1978). "Digital Bispectral Analysis of Self-Excited Fluctuation Spectra," *The Physics of Fluids*, vol. 21, pp. 1452-1453.

Kim, S. B. and Powers, E. J. (1995). "Estimation of Volterra kernels via higher-order statistical signal processing," in *Higher order statistical signal processing*, (Boashash, Powers, and Zoubier, eds.), Ch. 7, pp. 213-267, 1995.

Kravtchenko-Berejnoi, V. et al. (1995). "On the use of tricoherent analysis to detect nonlinear wave-wave interactions," Signal Processing, vol. 42, pp. 291-309.

Lii, K. S. (1982). "Non-Gaussian ARMA model identification and estimation," Proceedings of Business and Economics Statistics, ASA, pp. 135-141.

Mendel, J. M. (1988). "Use of Higher Order Statistics in Signal Processing and System Theory: An Update," *Proceedings of SPIE, Advanced Algorithms and Architectures for Signal Processing III*, vol. 975, pp. 126-144.

MIT/BIH (1997) *MIT/BIH Database: ECG Database Applications Guide*, 10th Edition. Harvard-MIT Division of Health Sciences and Technology, MIT Room 20A-113, Cambridge, MA 02139, USA.

Nagata, Y. (1970). "Lag joint probability, higher-order covariance function and higher-Order spectrum," Bulletin de la socie'te' Franco-Japonaise d'oceanographic, vol. 8, Part 2, pp. 78-94, May.

Nam, S. W.; Powers, E. J. (1994). "Application of Higher Order Spectral Analysis to Cubically Non-Linear System Identification," IEEE Transaction on Signal Processing, vol. 42, No. 7, pp. 1746-1765, July.

Nikias, C. L. (1988). "ARMA bispectrum approach to nonminimum phase system identification," *IEEE Transaction on Acoustics, Speech, and Signal Processing*, vol. ASSP-36, pp. 513-524, April.

Nikias, C. L.; Petropulu, A. P. (1993). *Higher Order Spectra Analysis: A Nonlinear Signal Processing Framework*, Prentice Hall.

Nikias, C. L. and Raghuveer, M. R. (1987). "Bispectrum estimation: A digital signal processing framework," *IEEE Proceedings*, vol. 75, No. 7, pp. 869-891, July.

Raghuveer, M. R. and Nikias, C. L. (1986). "Bispectrum estimation via parametric modeling," Signal Processing, Special issue on modern trends of spectral analysis, vol. 10, pp. 35-48, Jan.

Rizk, M., Zgallai, W. A., Carson, E., MacLean, A., & Grattan, K. (2002). "Multi-fractility in Fetal Heart Beat Dynamics," The *2nd European Medical and Biological Engineering Conference*, Austria, December.

Rizk M., Zgallai W. A., McLean, A., Carson, E., and Grattan, K. (2001) Virtues and Vices of Source Separation Using Linear Independent Component Analysis for Blind Source Separation of Non-linearly Coupled and Synchronised Fetal and Mother ECGs. *IEEE Engineering in Medicine and Biology Conference*, USA.

Rizk, M. et al. (2000) Novel decision strategy for P-wave detection utilising nonlinearly synthesised ECG components and their enhanced pseudospectral resonances. *IEE Proceedings Science, Measurement & Technology*, Special section on Medical Signal Processing, vol. 147, No. 6, pp. 389-397, November

Rizk M. and Zgallai, W. (1999) "Higher Order Statistics Are Indispensable Tools in The Analysis of Electrocardiogram Signals," IEE Colloquium on Statistical Signal Processing, January.

Rizk, M. et al. (1998) "Higher-Order Ambulatory Electrocardiogram Identification and Motion Artefact Suppression With Adaptive Second- and Third-Order Volterra Filters," SPIE '98 Adv Sig Proc Algorithms, Arch, & Implementations VIII Vol. 3461 pp. 417-431, USA, 19-24 July.

Rizk, M., Romare, D., Zgallai, W. A., Grattan, K., Hardiman, P., and O'Riordan, J. (1995) "Higher order statistics (HOS) in signal processing: Are they of any use?," IEE Colloquium, digest #111, pp. 1/1-1/6, London, May.

Rosenblatt, M. (1985). *Statistical Sequences and Random Fields*, Birkhauser, USA.

Rosenblatt, M. (1983). "Cumulants and Cumulant Spectra," in *Handbook of Statistics*, vol. 3, (D. Brillinger, and P. Krishnaiah, eds.), Amesterdam, Holland, pp. 369-387.

Subba Rao, T. (1983). "The Bispectral Analysis of Nonlinear Stationary Time Series with Reference to Bilinear Time Series Models," in *Handbook of Statistics*, vol. 3, (D. Brillinger, and P. Krishnaiah, eds.), Amesterdam, Holland, pp. 293-319.

Zgallai, W. A. (2012 a) Detection and Classification of Adult and Fetal ECG Using Recurrent Neural Networks, Embedded Volterra and Higher-Order Statistics, in *Recurrent Neural Networks*, El Hefnawi, M. and Mysara, M., Ed., InTech Open, ISBN 979-953-307-546-3.

Zgallai, W. A. (2012 b) Non-Invasive Fetal Heartbeat Detection Using Bispectral Contour Matching. The International Conference on Electronics and Biomedical Engineering Applications, Dubai, UAE, 7-8 January.

Zgallai, W. A. (2010). "Non-invasive fetal heartbeat detection using third-order cumulant slices matching and ANN classifiers," *The 7th International Association of Science and Technology for Development (IASTED), International Conference on Biomedical Engineering, IASTED*, Austria, 17/02.

Zgallai, W. A. (2009) Embedded Volterra for Prediction of Electromyographic Signals During Labour. *The 16th IEEE International Conference on Digital Signal Processing (DSP)*, Greece, 05/07.

Zgallai, W. A. (2007) *Advanced Robust Non-Invasive Fetal Heart Detection Techniques During Active Labour Using One Pair of Transabdominal Electrodes*, PhD Thesis, City University London, UK.

Zgallai, W. A. Et al., (1997) MUSIC-Based Bispectrum Detector: A Novel Non-Invasive Detection Method For Overlapping Fetal and Maternal ECG Signals. *Proceedings 19th IEEE International Conference Engineering in Medicine and Biology*, EMBS, pp. 72-75, USA, October.

Zgallai W. A. et al., (1997) Third-order cumulant signature matching technique for non-invasive fetal heart beat identification. *IEEE International Conference on Acoustics, Speech, and Signal Processing (ICASSP)*, vol. 5, pp 3781-3784, Germany.

Zurbenko, I. G. (1982). *The spectral analysis of time series*, Ch. 6, North-Holland Series in Statistics and Probability, vol. 3, pp. 169-176.